

Non-linear motions of Australian geodetic stations induced by non-tidal ocean loading and the passage of tropical cyclones

A. Mémin · C. Watson · I. D. Haigh ·
L. MacPherson · P. Tregoning

Received: 2 August 2013 / Accepted: 22 May 2014 / Published online: 12 June 2014
© Springer-Verlag Berlin Heidelberg 2014

Abstract We investigate daily and sub-daily non-tidal oceanic and atmospheric loading (NTOAL) in the Australian region and put an upper bound on potential site motion examining the effects of tropical cyclone Yasi that crossed the Australian coast in January/February 2011. The dynamic nature of the ocean is important, particularly for northern Australia where the long-term scatter due to daily and sub-daily oceanic changes increases by 20–55 % compared to that estimated using the inverted barometer (IB) assumption. Correcting the daily Global Positioning System (GPS) time series for NTOAL employing either a dynamic ocean model or the IB assumption leads to a reduction of up to 52 % in the weighted scatter of daily coordinate estimates. Differences between the approaches are obscured by seasonal variations in the GPS precision along the northern coast. Two compensating signals during the cyclone require modelling at high spatial and temporal resolution: uplift induced by the

atmospheric depression, and subsidence induced by storm surge. The latter dominates (> 135 %) the combined net effect that reaches a maximum of 14 mm, and 10 mm near the closest GPS site TOW2. Here, 96 % of the displacement is reached within 15 h due to the rapid transit of cyclones and the quasi-linear nature of the coastline. Consequently, estimating sub-daily NTOAL is necessary to properly account for such a signal that can be 3.5 times larger than its daily-averaged value. We were unable to detect the deformation signal in 2-hourly GPS processing and show that seasonal noise in the Austral summer dominates and precludes GPS detection of the cyclone-related subsidence.

Keywords Non-tidal ocean loading · Storm surge loading · Global positioning system · Australia

A. Mémin (✉)

School of Physical Sciences, University of Tasmania, Private bag 37, Hobart, TAS 7001, Australia
e-mail: anthony.memin@utas.edu.au

C. Watson

School of Land and Food, University of Tasmania, Private bag 76, Hobart, TAS 7001, Australia

I. D. Haigh

Ocean and Earth Science, National Oceanography Centre, University of Southampton, European way, Southampton SO14 3ZH, UK

L. MacPherson

School of Environmental Systems Engineering and the UWA Oceans Institute, The University of Western Australia, 35 Stirling Highway, Crawley, WA 6009, Australia

P. Tregoning

Research School of Earth Sciences, The Australian National University, Canberra, ACT 0200, Australia

1 Introduction

Mass loads on Earth vary in both space and time. In response to this continuous redistribution of mass, the surface of the Earth deforms in three dimensions. The resulting deformations can be observed through space geodetic observing systems including global navigation satellite systems (GNSS), very long baseline interferometry (VLBI), satellite laser ranging (SLR) and Doppler orbitography and radiopositioning integrated by satellite (DORIS). Such surface deformation is one phenomenon that causes departures in site coordinates from the idealized linear motion that is driven by plate tectonics and underpins the terrestrial reference frame (TRF). Correcting observations for the deformation induced by well-described phenomena should result in an improved TRF (Petit and Luzum 2010), and thus improve the ability to make geophysical interpretation from the residual signal observed in geodetic time series.

Typical mid-latitude displacements of the Earth surface induced by non-tidal atmospheric pressure loading (NTAL) can be as large as 20 mm (e.g. [van Dam and Wahr 1987](#)) but they can reach 30 mm at higher latitudes ([Schuh et al. 2003](#)). When computing deformation induced by NTAL, one needs to take into account the ocean response to atmospheric pressure variations. The inverted barometer (IB) hypothesis (i.e. assuming that the sea surface entirely adjusts to atmospheric fluctuations) is appropriate for periods longer than 5–20 days and is usually employed (e.g. [van Dam and Wahr 1987](#); [van Dam and Herring 1994](#); [van Dam et al. 1994](#); [Petrov and Boy 2004](#); [Tregoning and van Dam 2005](#); [Tregoning et al. 2009](#)). However, the IB assumption is not valid for shorter periods (e.g. [Wunsch 1972](#); [Tierney et al. 2000](#); [Wunsch and Stammer 1997](#)) at which important ocean changes can still occur. [Petrov and Boy \(2004\)](#) showed that coastal and island stations are the most affected by the differences in the estimated displacements when using an IB and a non-IB ocean response. [van Dam et al. \(2012\)](#) confirmed this result by comparing weekly GPS solutions with predicted ocean bottom pressure changes from the estimating the circulation and climate ocean (ECCO) project ([Stammer et al. 2002](#)). They also showed that not only coastal and island sites but also inland sites are affected by a redistribution of the ocean's internal mass. Using the ECCO and regional ocean models, [Williams and Penna \(2011\)](#) showed that displacements induced by non-tidal ocean loading (NTOL) around the southern North Sea are as large as that due to NTAL and that the combined correction can lead to a RMS reduction of daily coordinate time series in the vertical component of about 20–30%. [Williams and Penna \(2011\)](#) and [van Dam et al. \(2012\)](#) have also shown that correction for the NTOL signal can decrease the variance in the vertical component at the majority of sites in their respective study regions. More specifically, [Williams and Penna \(2011\)](#) have obtained a greater variance reduction using their high-resolution ocean model than using the global ECCO model (kf066b). The ECCO model has a 12-hourly temporal resolution and a spatial resolution of 0.3° – 1° and may not be able to appropriately capture sub-daily ocean changes that deviate from the IB ocean's response (see Sect. 2.2).

Australia has been improving its geodetic network through the development of the AuScope network ([Coleman et al. 2008](#)). This network includes VLBI and GNSS sites spread over the Australian continent, as well as upgrades to SLR observatories. Its primary aim is not only to investigate intraplate strain but also to improve the Australian contribution to the TRF. Australia is surrounded by oceans, which make it sensitive to deformations induced by tidal ocean loading and NTOL. The northern coast is also subject to large storm surge events induced by tropical cyclones that are likely to introduce frequent non-linear behaviour in coordinate time series. Geodetic time series are not currently routinely cor-

rected for NTOL (including the effects of storm surge). Storm surges are characterized by sub-daily oceanic behaviour that deviates from the typical IB response and can substantially deform the Earth surface. For instance, [Fratepietro et al. \(2006\)](#) predicted a subsidence of up to 20–30 mm at some geodetic sites around the southern part of the North Sea in response to a typical storm surge. [Geng et al. \(2012\)](#) successfully detected a storm surge loading event in the same area in sub-daily (2 hourly) global positioning system (GPS) position estimates. In this case, the storm surge caused station displacements of up to a few centimetres within a few hours, above the typical noise threshold in sub-daily GPS processing. While storm surge magnitudes around Australia may be smaller and less prolonged than those influenced by the semi-enclosed nature of the geometry in the North Sea as studied by [Geng et al. \(2012\)](#), it is important to quantify the magnitude and potential influence of NTOL on geodetic time series across the Australian continent, to ensure the most accurate contribution of the Australian network to the TRF.

We examine the effects of daily and sub-daily ocean and atmosphere variations on the predicted vertical motions at Australian geodetic sites. In particular, we investigate the loading deformation induced during the passage of a tropical cyclone over Australia's tropics as a tool to elucidate an upper bound on the magnitude of sub-daily loading effects. These rapid ocean variations deviate from the IB ocean's response to atmospheric pressure changes and their effect on geodetic time series from the Australian GNSS network is investigated.

Following an analysis of the spatial and temporal distribution of the predicted non-tidal atmospheric and ocean deformations spanning the network from January 2002 to December 2010 (Sect. 2), we investigate the predicted non-linear motion induced by the storm surge caused by tropical cyclone Yasi which crossed the coast line between Cairns and Townsville (northwestern Australia) in February 2011 (Sect. 3). We subsequently detail the geodetic observations used (Sect. 4.1) to compare predicted vertical displacements with observed geodetic time series. We discuss our results for daily solutions (Sect. 4.2) and also investigate the possible detection of Yasi in sub-daily geodetic solutions (Sect. 4.3). Our concluding remarks follow in Sect. 5.

2 Vertical motion induced by non-tidal oceanic and atmospheric loading (NTOAL) at geodetic sites in Australia

To compute the motion of a geodetic site induced by changes in the atmosphere and the ocean, one has to deal separately with the changing mass loads occurring over the land and those over the ocean. The loading over the land may be estimated using surface pressure fields output from global

atmospheric models. Over the ocean, an assumption regarding the ocean's behaviour to the change in air pressure is required, and the effects of ocean dynamics may also need to be considered.

2.1 Non-tidal atmospheric loading using the IB hypothesis

As introduced in Sect. 1, the IB ocean response to changes in atmospheric pressure is the most commonly used assumption for computing NTAL. This response is directly derived from the atmospheric model assuming that air pressure variations are entirely compensated by static ocean height changes (e.g. van Dam and Wahr 1987; Boy and Lyard 2008). It results in a uniform pressure over the oceans that is due to the net change of air mass above the oceans (van Dam and Wahr 1987). The combination of loading induced by atmospheric pressure over the lands and over the oceans, through the IB hypothesis, leads to what we term IB-NTAL (Table 1). Note that this implies the tidal component of the mass load or deformation signal is removed (e.g. Tregoning and van Dam 2005).

We use the surface pressure field of the latest global atmospheric reanalysis released by the European Centre for medium-range weather forecasts (ECMWF), namely the ERA-interim model (Dee et al. 2011), to compute the loading induced by air pressure variations. We use a mixture of analysis and forecast surface pressure fields which allows a 3-hourly output on a regular grid with a 1.5° spatial sampling (http://data-portal.ecmwf.int/data/d/interim_daily/). This temporal resolution enables the comparison of the IB-NTAL with the loading estimated using the dynamic ocean model introduced in Sect. 2.2. To compute the IB-NTAL, we remove at each site tidal atmospheric loading by performing a monthly harmonic analysis of loading time series data, removing diurnal (S1), semi-diurnal (S2) and ter-diurnal (S3) constituents. This approach removes more of the periodic signals than the approach of Petrov and Boy (2004) through the use of monthly means, and we verified that this approach leads to effectively the same results as per other filtering strategies (e.g. Tregoning and Watson 2009).

2.2 Non-tidal oceanic and atmospheric loading using a dynamic ocean model

If one wants to determine the loading induced by the dynamic non-tidal behaviour of the ocean (D-NTOL, see Table 1), one has to employ an ocean model to take into account changes over the oceans. We use the barotropic, non-linear and time-stepping hydrodynamic Toulouse Unstructured Grid Ocean model (TUGO-m) to compute the D-NTOL. TUGO-m is an update of the previous 2D gravity wave model MOG2D (Carrère and Lyard 2003) and provides non-tidal sea height variations with 3-hourly temporal resolution, and a global coverage on a regular 0.25° grid. Around the coast, the model

Table 1 Summary of the treatment over land and over ocean to derive the three different mass loads subsequently convolved to generate vertical displacement

Acronyms	Over land	Over ocean
IB-NTAL	ECMWF	ECMWF (IB)
D-NTOL	–	TUGO-m
D-NTOAL	ECMWF	ECMWF (NIB) + TUGO-m

NT Non tidal, *IB* inverse barometer, *NIB* non-inverse barometer, *AL* atmospheric loading, *OL* oceanic loading

employs a finite element grid with spatial resolution of a few kilometres (Carrère and Lyard 2003; Boy and Lyard 2008). TUGO-m is forced by air pressure and winds from the operational analysis of the ECMWF which has a finer resolution than the reanalysis model. TUGO-m only includes the barotropic dynamic effects of the oceans which is well suited for studying the variations at periods less than a month. Thus, this model differs from that employed by van Dam et al. (2012) which is an ocean general circulation model from the ECCO project. The ECCO model is a baroclinic model, forced by winds, daily heat and freshwater air–sea fluxes. TUGO-m has a finer temporal and spatial resolution than the ECCO model; hence, it is more suitable for studying the loading due to sub-daily variations of the oceans as is presented here. For comparison with daily GPS time series, we use both TUGO-m and ECCO models. However, given negligible differences, we focus on the results obtained using TUGO-m.

Validation of the MOG2D model, for which TUGO-m is the follow-on model, is described in Carrère and Lyard (2003). TUGO-m shows very good agreement with tide gauge data in the North Sea (Figs. 7 and 8 of Boy and Lyard (2008) and Fig. 4 of Boy et al. (2009)) and has already been used to decrease the variance of gravity and tilt measurements (e.g. Boy and Lyard 2008; Boy et al. 2009). TUGO-m is currently employed by the Groupe de Recherche de Géodésie Spatiale in Toulouse, France, to compute the space and time gravity field variations from the Gravity Recovery and Climate Experiment Mission (Lemoine et al. 2007; Bruinsma et al. 2010).

The total pressure acting on the solid Earth surface is equal to the NTAL over land and to the sum of the NTAL and D-NTOL over the ocean. The mass load used to compute D-NTOL is derived from multiplying the sea height variations from TUGO-m with the density of the sea water and the surface gravity. The NTAL component is computed from the surface pressure fields of the ECMWF model. Over the oceans, no assumption is made, meaning that for this computation we use the non-IB (NIB) ocean response to atmospheric changes. We add the NTAL to the D-NTOL to form the D-NTOAL (Table 1).

2.3 Computation method

To compute the vertical displacement associated with IB-NTAL, D-NTOL and D-NTOAL at sites within the Australian study region, we use the Green's functions approach of Farrell (1972) which has been widely applied in the literature (e.g. van Dam and Wahr 1987; Merriam 1992; Boy et al. 1998; Petrov and Boy 2004; Mémin et al 2009). For each geodetic site, this approach involves convolving the surface mass or pressure variation fields with the Green's functions for the vertical displacement. The Green's functions are computed according to Farrell (1972) using elastic Love numbers derived from the Preliminary Reference Earth Model (Dziewonski and Anderson 1981). The vertical displacements are obtained in the centre of figure reference frame.

2.4 Spatial and temporal signature of NTOAL

We first characterize the spatial and temporal differences of the signature of the predicted IB-NTAL and D-NTOAL signals at geodetic sites in Australia. We compute the time series of predicted changes in the vertical direction at the locations of 21 core geodetic GNSS sites across Australia from January 2002 to December 2010. To compare with the observed daily geodetic time series introduced in Sect. 4.1, we run a daily average on the 3-hourly resulting loading time series. To compare the long-term scatter of the two time series (IB-NTAL and D-NTOAL) at each site, we first compute the standard deviation of each daily time series and then take their ratio (Fig. 1a). A ratio close to 1 indicates that the variability of the time series is barely affected by the choice of the model used. A ratio lower than 1 indicates that the IB-NTAL time series has a lower variability than the D-NTOAL series (and vice versa). As highlighted in Fig. 1a, these ratios mainly show the difference of the magnitude of the seasonal signals within IB-NTAL and D-NTOAL time series. The mean ratio across Australian sites is 0.98 (Fig. 1a). Eleven sites show ratios close to 0.9, seven close to 1.0 and three between 1.2 and 1.3 (Fig. 1a). The latter ratios are obtained at DARW, JAB2 and KAT1 on the northern coast and they reflect that the seasonal signal in IB-NTAL is larger than in D-NTOAL. Reciprocally, the IB-NTAL time series of the 11 sites, with a ratio lower than 1.0, has a lower seasonal signal than the D-NTOAL time series.

To determine the differences between the long-term scatter of the IB-NTAL and D-NTOAL time series induced by signals other than at seasonal timescale, we fit a model using least squares including periodic components at solar annual and semi-annual frequencies and remove it from the loading time series. It changes the mean ratio to 0.93 (Fig. 1b), with ten sites with a ratio close to 1.0, seven close to 0.9 and four close to 0.75–0.8. This indicates that at 11 sites, the

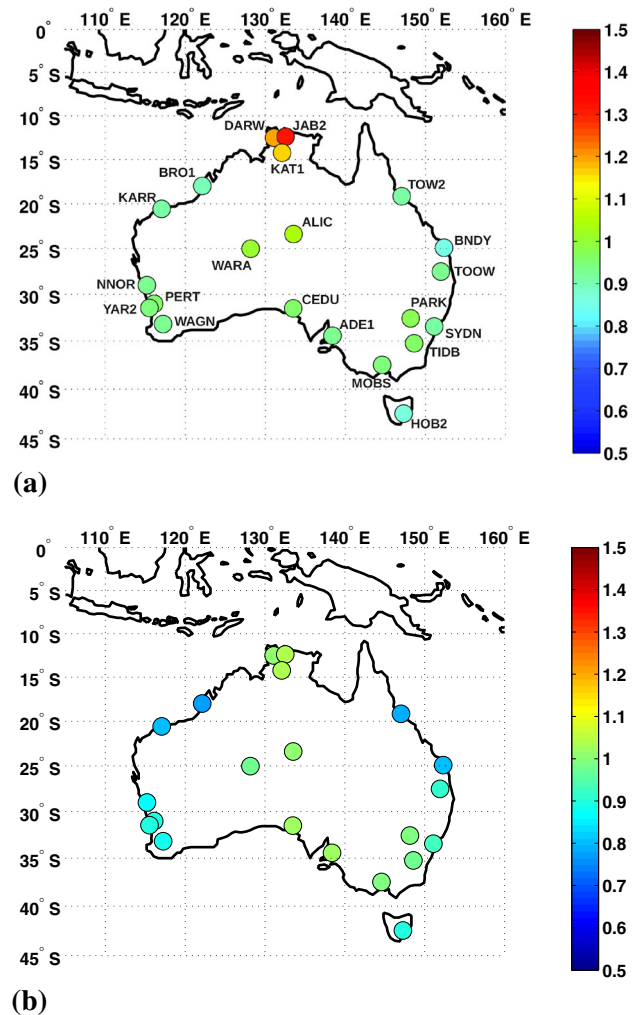


Fig. 1 Ratio of the long-term scatter of the daily values of the modelled vertical displacement induced by IB-NTAL with that induced by D-NTOAL before (a) and after (b) removing an annual and semi-annual signal

D-NTOAL has a long-term scatter, induced by signals below seasonal time scales, 10 to 20–25 % larger than the IB-NTAL. The lowest ratios are at KARR, BRO1, TOW2 and BNDY, on the northern coast of Australia. These locations are subject to increased ocean variability due to tropical depressions and cyclones.

Due to sub-daily variation in the predicted vertical site motion, we assign to each daily sample an uncertainty which is the sub-daily scatter of the IB-NTAL and D-NTOAL estimates for the corresponding day. To investigate the variability in the sub-daily scatter of IB-NTAL and D-NTOAL, we use a similar ratio, this time derived from the respective standard deviations of the sub-daily scatter time series. They are mapped in Fig. 2. The mean ratio is 0.84, 12 sites have a ratio between 0.9 and 1.0 and 9 have a ratio between 0.5 and 0.9. We find that using the IB assumption leads to sub-

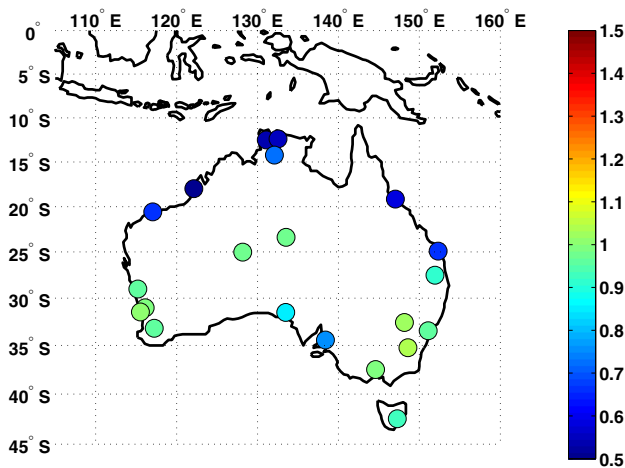


Fig. 2 Ratio of the variability in sub-daily scatter of the predicted vertical displacement induced by IB-NTAL with that induced by D-NTOAL

daily scatters with a systematically smaller time variability than that obtained using TUGO-m along the northern coast of Australia. There, we also obtain the largest differences where the assumption of an IB ocean response leads to sub-daily scatter variabilities that are up to 50–55 % smaller than those obtained using the dynamic response. The northern coast is well characterized by extensive shallow shelf margins with high-amplitude and high-frequency ocean dynamics. The dynamic response also leads to larger variabilities of the sub-daily scatter compared with the IB response at sites CEDU and ADE1 in southern Australia, adjacent to the Spencer Gulf and shallow shelves, showing that this region is subject to high-frequency ocean changes that are not adequately captured by the IB response.

Comparing Figs. 1b and 2, we see that sites such as ADE1 and CEDU with a long-term scatter ratio close to 1.0 present ratios close to 0.9 for the sub-daily scatter variability. In other words, those sites, where the long-term scatter of IB-NTAL and D-NTOAL time series are very similar, show different daily variations due to sub-daily differences between the two approaches. This difference is more evident for DARW, JAB2 and KAT1 where the sub-daily scatter variability ratios are about 0.5, 0.55 and 0.75, respectively. The weighted standard deviations of the daily D-NTOAL time series, with seasonal signals removed, range between 0.8 mm at JAB2 and DARW and 1.9–2.0 mm at ADE1, CEDU and MOBS. IB-NTAL time series shows only slight differences (<20–25 %). Therefore, we do not expect important differences between the reductions of the weighted variance of the daily geodetic time series when corrected for D-NTOAL or IB-NTAL.

Sub-daily scatter of the predicted IB-NTAL and D-NTOAL time series can be significantly different along the northern coast of Australia where the largest storm surge events occur (Haigh et al. 2014a, b), mainly driven by tropical cyclones. To determine an upper bound on sub-daily move-

ment, we now investigate the predicted deformation induced from a major tropical cycle (category 5 cyclone Yasi) and its associated storm surge. Yasi was the biggest cyclone recorded in Queensland in almost 100 years (<http://www.bom.gov.au/cyclone/history/yasi.shtml>). Following the development of the modelling for this high-frequency event, we investigate both daily and sub-daily observed displacements in GPS time series.

3 High-frequency vertical loading: NTOL induced by a cyclone-induced storm surge

3.1 Tropical cyclone Yasi

Tropical cyclones are rapid events that can produce large storm surges, and each year, the northern coast of Australia is subject to 11 tropical cyclones on average, 4 of which make landfall. Tropical cyclones are strong atmospheric depressions which induce an uplift of the surface through atmospheric pressure unloading as well as a subsidence caused by oceanic loading from storm surges that may reach several metres. Figure 3 shows the surface pressure along the track of cyclones which occurred in January and February 2011. We investigate tropical cyclone Yasi that occurred between January 29 and February 3 in 2011. The lowest measured surface pressures were ~930 hPa on February 2, causing a pressure change along its track of ~75 hPa (<http://australiasevereweather.com/cyclones/>). The surge induced by the passage of Yasi reached more than 5 m at Cardwell along the coastline of northern Queensland, and more than 2 m at Townsville (Haigh et al. 2014b).

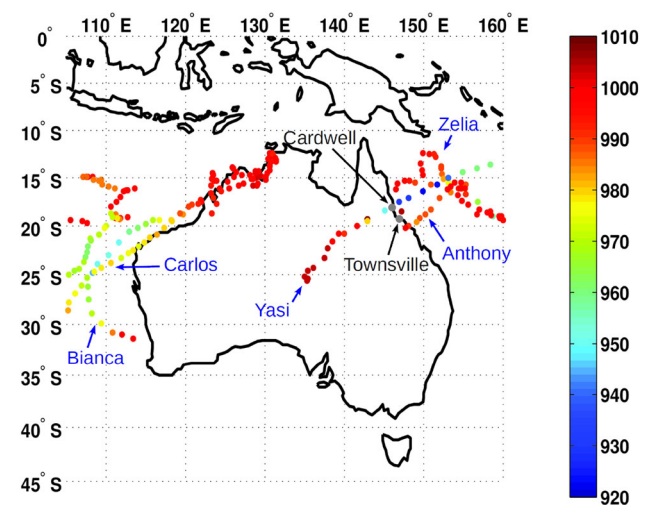


Fig. 3 Surface pressures (hPa) along tropical cyclone tracks for January and February 2011 from <http://australiasevereweather.com/cyclones>. Names of cyclone are in blue and dots spacing is ~6 h

3.2 Loading predicted by TUGO-m

To provide an initial point of comparison, we use the global ocean model TUGO-m to quantify the effect of the surge caused by Yasi on the vertical displacement as would be experienced by the GPS station TOW2 located in Townsville, the sole permanent station in this region. The predicted 3-hourly changes in the vertical coordinate due to the oceanic and the atmospheric loading (D-NTOAL) during the passage of Yasi are shown by the green curve in Fig. 4. The corresponding daily-averaged time series, computed using the mean of the eight 3-hourly values centred on 12:00 of the 24-h time interval, is the dashed curve of the same colour. A minimum is obtained at the vertical black line which corresponds to the date at which Yasi approximately reached the coast and started to move over land. At this time, the model predicts a subsidence of the station of ~ 3 mm in 12–15 h. It shows that the maximum displacement is obtained when Yasi reaches the coast, namely when the storm surge is maximum.

The blue curve in Fig. 4 corresponds to the predicted vertical displacement at TOW2 obtained using the IB assumption for the ocean's response to the atmosphere changes, namely the IB-NTAL effect. Contrary to the displacement induced by the D-NTOAL, the IB-NTAL leads to a maximum displacement with a magnitude of $+1.6$ mm after the cyclone has reached the coast (vertical black line). This corresponds to the uplift induced by the maximum atmospheric depression over land. We can also see that, while the surface is subsiding due to D-NTOAL, it is rising in response to IB-NTAL. This reflects that, during this storm, the subsidence induced by the D-NTOL (the red curve in Fig. 4) is dominant over the uplift caused by the unloading of the atmosphere.

When the cyclone reaches the coastline, two opposite effects that compensate take place: the ground uplifts because

of the atmospheric depression and subsides due to the ocean surge. At the time Yasi reaches the coastline, the predicted vertical displacement at TOW2 is 1.0, -3.2 and -4.6 mm, according to IB-NTAL, D-NTOAL and D-NTOL models, respectively (Fig. 4). Also at this time, the D-NTOL and IB-NTAL predicted uplifts (red and blue curves in Fig. 4) represent about 140 and -30% of the D-NTOAL predicted uplift (green curve in Fig. 4), respectively. This results in a relative difference of 4.2 mm between the displacement induced by IB-NTAL and that induced by D-NTOAL. The two resulting time series are consequently significantly different when Yasi is close to the coast.

3.3 Loading predicted using a high-resolution ocean model

TUGO-m, which has a resolution of 0.25° , is likely to be too coarse to reliably capture the space and time signature of storm surge events induced by tropical cyclones (e.g. Williams and Penna 2011). To investigate this we use the surge component of a regional ocean model recently developed by Haigh et al. (2014a, b) around Australia. It is a depth-averaged barotropic hydrodynamic model with a resolution of between 1/3rd and 1/5th of a degree (~ 20 and 80 km) at the open tidal boundaries, increasing to 1/12th of a degree (~ 10 km) along the entire coastline of mainland Australia, Tasmania and surrounding islands (Haigh et al. 2014a). The model has been forced with mean sea level pressure fields and wind fields from the US National Center for Environmental Predictions/National Center for Atmospheric Researchs (NCEP/NCAR) global reanalysis (Kalnay et al 1996). As for TUGO-m, the temporal (6 hourly) and spatial (2.5°) resolution of the NCEP/NCAR forcing is sufficient for predicting storm surges associated with large extra-tropical storms, but is too coarse to accurately predict the more intense and

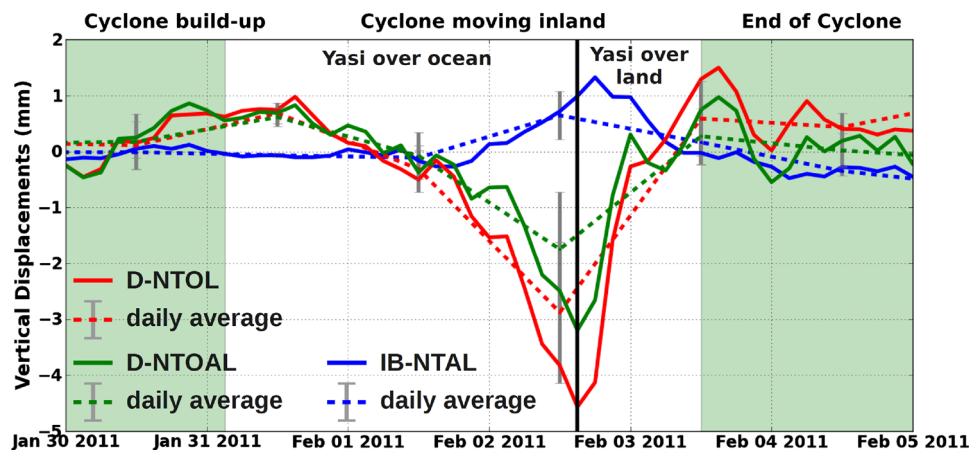
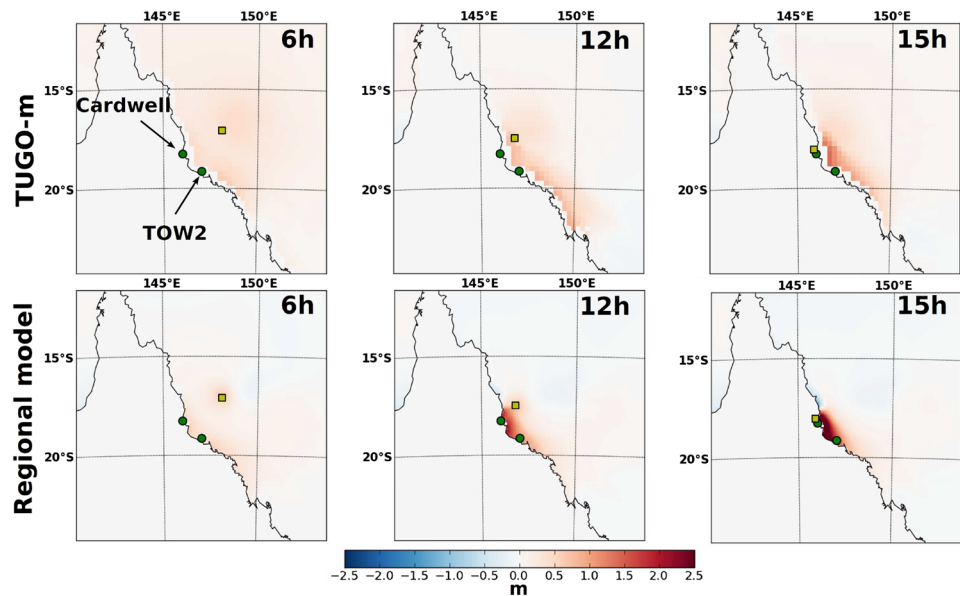


Fig. 4 Predicted changes in the vertical coordinate of the GPS station TOW2 (Townsville) due to the storm surge induced by the tropical cyclone Yasi considering the 3-hourly D-NTOL (red), D-NTOAL (green) and the IB-NTAL (blue). Dash lines are daily-averaged time

series where errors are given by grey bars. The black line indicates when Yasi approximately reaches the main land. White part of the plot corresponds to the Bureau of Meteorology of Australia warnings, and to the formation and eventual reduction of Yasi

Fig. 5 Change in the ocean heights (m) as predicted by TUGO-m and the surge component of the regional ocean model of Haigh et al. (2014b) on February 2, 2011, at 6, 12 and 15 h. The green dots show the location of Cardwell and the TOW2 GPS station. The yellow squares show the centre of the cyclone



localized tropical cyclone-induced storm surge events. To overcome this, statistical models of tropical cyclone behaviour have been developed using an analysis of tide gauge records around Australia (Haigh et al. 2014b). Wind and pressure fields derived for synthetic events were used to drive a hydrodynamic model of the Australian continental shelf region configured by Haigh et al. (2014a) and to predict the associated storm surge. A 0.1° rectilinear grid was built throughout the domain, and to better resolve flow in the near-shore region, the grid was refined to 0.05° (Haigh et al. 2014b). For Yasi, the measured and predicted surge at four sites along the northeastern Australian coast (Cape Ferguson, Townsville, Cardwell, Clump Point) shows very good agreement (Fig. 6 of Haigh et al. 2014b). For example, the 5.5-m surge observed at the Cardwell tide gauge (mid-way between Cairns and Townsville) is reproduced to within 8 cm. We only use the surge component for Yasi to determine the localized loading effects at TOW2 induced by the subsequent storm surge, remeshing the native unstructured grid to a regular grid spacing of 0.05°.

To see how the estimated ocean loading can be affected by the two ocean models, we map the predicted variation in ocean heights (Fig. 5) during February 2, 2011 at 6, 12 and 15 h, when the tropical cyclone arrived close to the coast and produced the largest change in ocean heights. Despite the maximum surge recorded at Cardwell (5.5 m, Fig. 6) we bound the colour scale in Fig. 5 to -2.5 and 2.5 m to emphasize the difference between the two ocean models with time. The spatial feature of Yasi in the ocean is broader using TUGO-m compared to the surge component of the regional model which shows localized sea level elevation changes. This changes both the spatial and temporal characteristics of the subsequent predicted loading signal. The magnitude of the change in ocean heights is lower for TUGO-m than

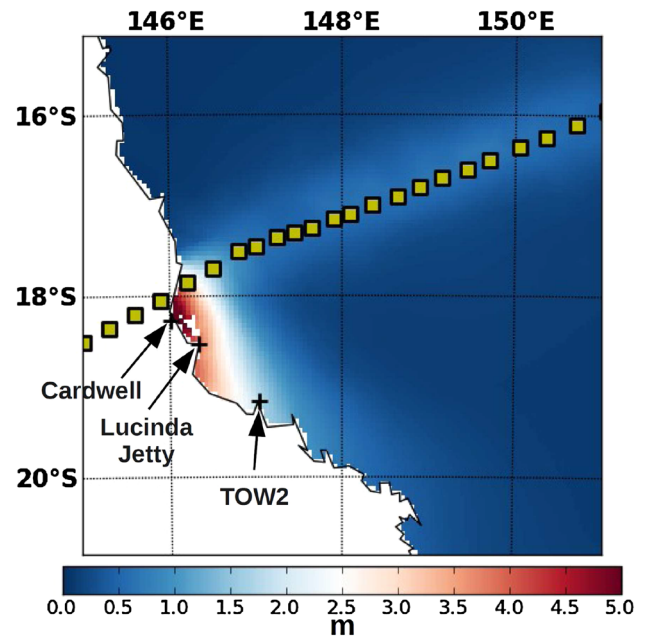


Fig. 6 Maximum water height induced by the surge during the passage of Yasi predicted by the regional model of Haigh et al. (2014b). The yellow squares show the cyclone track at 1-h intervals

for the regional model which subsequently would induce a larger localized loading signal for the latter model. Similarly, the spatial location of the maximum loading is located further North (closer to Cardwell) for the regional model. Following the passage of the cyclone over land, the regional model shows subsidence of the ocean surface not visible in the TUGO-m predictions. Finally, the coastline definition in TUGO-m is coarser than that used in the regional model, resulting in a greater distance between the closest GPS site (TOW2) and the ocean.

Fig. 7 Predicted changes in the vertical coordinate of the TOW2 GPS station induced by D-NTOL (a) and D-NTOAL (b) during the passage of Yasi using the global ocean model TUGO-m (red and green) and the regional model of Haigh et al. (2014b) (black and magenta)

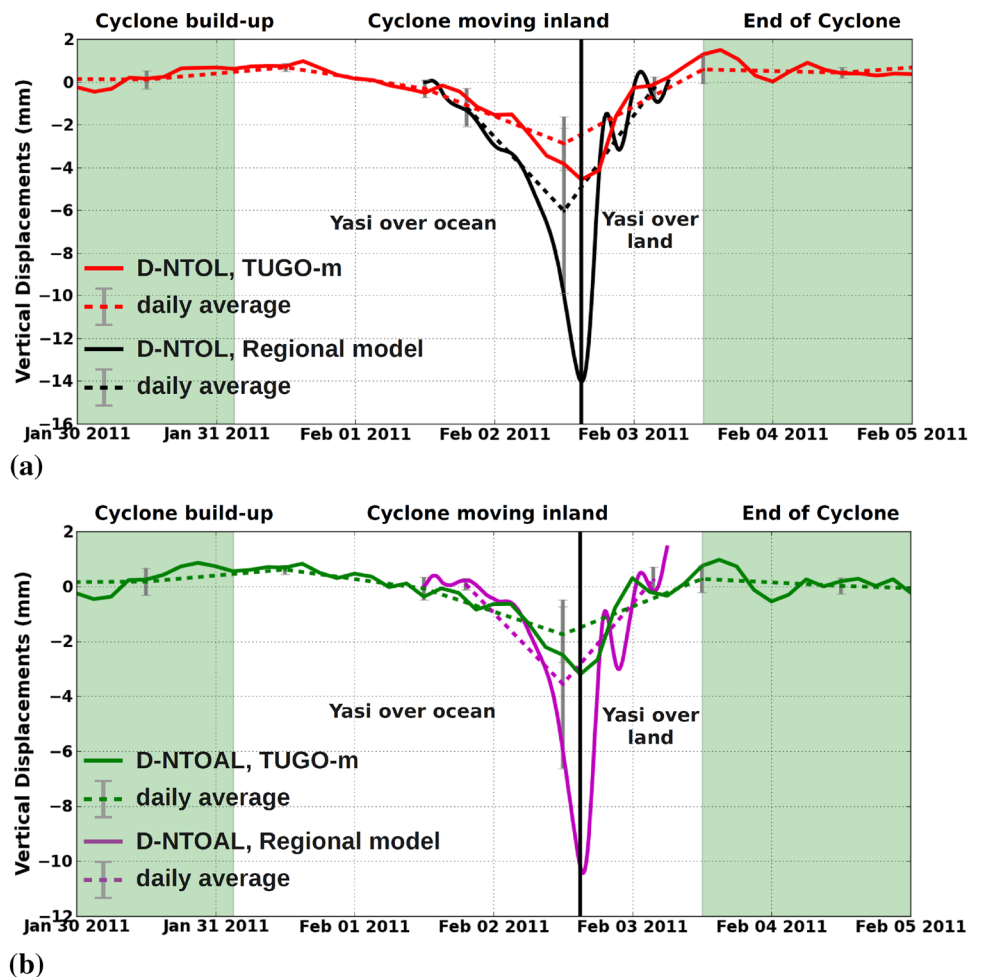


Table 2 Maximum and daily average of the vertical displacement induced by IB-NTAL, D-NTOL and D-NTOAL at Cardwell, Lucinda Jetty and TOW2 on February 2, 2011

Site	IB-NTAL		D-NTOL				D-NTOAL			
	TUGO-m		TUGO-m		Regional		TUGO-m		Regional	
	Max.	Mean ± STD	Max.	Mean ± STD	Max.	Mean ± STD	Max.	Mean ± STD	Max.	Mean ± STD
Cardwell	2.8	1.3 ± 0.8	-3.3	-2.0 ± 0.9	-12.0	-4.1 ± 3.3	-1.1	-0.4 ± 0.6	-6.2	-1.1 ± 2.0
Lucinda Jetty	2.5	1.1 ± 0.7	-4.4	-2.6 ± 1.2	-19.1	-6.5 ± 5.5	-2.5	-1.1 ± 0.8	-14.0	-3.6 ± 4.3
TOW2	1.6	0.7 ± 0.4	-4.6	-2.9 ± 1.3	-14.0	-6.0 ± 3.9	-3.2	-1.8 ± 1.0	-10.4	-3.6 ± 3.1

D-NTOL and D-NTOAL are computed using TUGO-m and the regional model, Units are mm
 STD Standard deviation

To illustrate these effects in time, Fig. 7 shows the time series for the vertical displacement induced by D-NTOL and D-NTOAL at TOW2, predicted using the variation of ocean heights from the two models. The regional model predicts a vertical displacement range of 14.0 and 10.4 mm for D-NTOL and D-NTOAL, respectively (Table 2) while TUGO-m predicts about one-third of this amplitude (4.6 and 3.2 mm, respectively). The smaller change predicted by TUGO-m is likely to involve contributions from the spatial

resolution and the coastline definition. Reducing the resolution of the regional model to 0.25° using linear interpolations to compute D-NTOL at TOW2 for comparison purposes decreases the amplitude of the vertical motion of TOW2 to 9 mm, which represents a reduction of 36%. The coastline definition modifies the location of the ocean loading which is systematically further away from TOW2 and consequently further attenuates the vertical displacement due to NTOL.

The Yasi surge signal has a longer duration in the global model than in the regional model, which shows that most of the loading occurs during 1 day, February 2, 2011 (Fig. 7). On this day, according to the regional model, the station returns to its nominal position within about 18–24 h, undergoing a 11- and 10-mm vertical displacement due to D-NTOL and D-NTOAL, respectively. In the same time span, a maximum predicted displacement of 16.5 (D-NTOL) and 14.0 mm (D-NTOAL) was found ~60 km South of Cardwell, and ~140 km North of TOW2, at Lucinda Jetty ($18^{\circ} 31' 26''\text{S}$, $146^{\circ} 19' 51''\text{E}$, Fig. 6). At this location the total predicted vertical displacement due to D-NTOL is 19.1 mm (Table 2). Figure 6 shows the maximum water height predicted during the passage of Yasi. It shows that TOW2 is located within the southern limit of the surge while Lucinda Jetty is closer to the centre of the bulge formed during the surge. Even though TOW2 is surrounded by a larger amount of water than Lucinda Jetty, the loading is less important because TOW2 is further away from the main bulge. However, at the maximum surge location, close to Cardwell, the predicted vertical displacements due to D-NTOL and D-NTOAL are reduced to 12.0 and 6.2 mm, respectively, given the variation in geometry and presence of a near-shore island in this vicinity. Conceptually, this is in agreement with Geng et al. (2012), who show that the amplitude of motion of a geodetic site due to a surge loading depends on not only the distance to the nearest coast, but also to the shape of the coastlines and the surrounding land-sea distribution.

The vertical displacements predicted at Cardwell, Lucinda Jetty and TOW2 are lower than those predicted and observed by Geng et al. (2012) at sites with a similar configuration (e.g. GORE, LOWE, ALDB) in the North Sea during a storm surge that occurred on November 9 2007, despite their predicted storm surge showing broadly lower maximum surge heights. The difference in the amplitude of the predicted vertical displacement is a direct consequence of the difference in the geometry of the North Sea and that of the northeastern Australian coast. The North Sea is a semi-enclosed bay, roughly about 500 km wide, in which outflow is significantly restricted compared with our studied region which is characterized by a quasi-linear coastline. This results in the surge in the North Sea having a wider spatial extension and longer duration, leading to prolonged loading effects.

4 Application to geodetic time series

4.1 Data

To assess if the root mean square (RMS) of the geodetic time series can be reduced a posteriori by applying the predicted daily D-NTOAL vertical displacements, we use the daily GPS time series solutions from the Australian National Uni-

versity (ANU) for the time interval January 2002–December 2010, updated from Tregoning and Watson (2009). The GPS analysis is undertaken in the GAMIT/GLOBK (10.38) suite (Herring et al. 2010) and includes correction at the observation level for both tidal atmospheric loading and IB-NTAL (Tregoning and van Dam 2005; Tregoning and Watson 2009, 2011). IB-NTAL corrections are estimated using the NCEP reanalysis products (Tregoning and van Dam 2005; Tregoning and Watson 2009). The solutions use the latest atmospheric mapping function (VMF1) with a priori estimates of zenith hydrostatic delay derived from the ECMWF meteorological reanalysis fields. Standard body tide and loading corrections are applied according to the International Earth Rotation and Reference Systems Service (IERS2010) standards (solid earth tide, ocean tide loading and pole tide loading, see Petit and Luzum 2010).

Our time series analysis of the GPS data involves a two-stage process to mitigate the influence of outliers. Pre-processing involves removal of all data with uncertainty estimates exceeding a threshold of 16 mm. This eliminates typically $\leq 7\%$ of data for each individual time series, and is usually indicative of daily estimates with significant tracking outages over the course of a 24-h observation session. To investigate the effect of high-frequency D-NTOAL, we remove the low-frequency energy contained at the seasonal periods. We fit a model that includes mean offset, trend, periodic components and time-dependent jumps using the method of weighted least squares. The periodic component includes terms to fit solar annual and semi-annual periods, as well as harmonics 1–6 of the GPS draconitic year (~ 351.4 days), shown to be a source of anomalous energy in GPS time series (Ray et al. 2008; Tregoning and Watson 2009). We are unable to resolve both the solar and the draconitic annual terms given the time series length; however, this is not problematic given that the goal here is merely to attenuate any signal at these low frequencies. To remove remaining outliers, we iterate this fitting procedure but discard samples with a normalized residual from the previous fit greater than 2 (typically $\leq 10\%$ of the selected data).

4.2 Data residuals

To generate a GPS time series corrected for the effects of D-NTOAL and given that the GPS analysis strategy employed applies IB-NTAL at the observation level, we first must restore a daily-averaged value of IB-NTAL to have a solution where the atmospheric pressure loading is not mitigated by an IB response of the ocean. Adding or removing a daily-averaged value of atmospheric pressure loading has been found to be the same as applying it at the observation level to within 0.1 mm (Tregoning and Watson 2009). Figure 8 shows the resulting weighted standard deviations for each site.

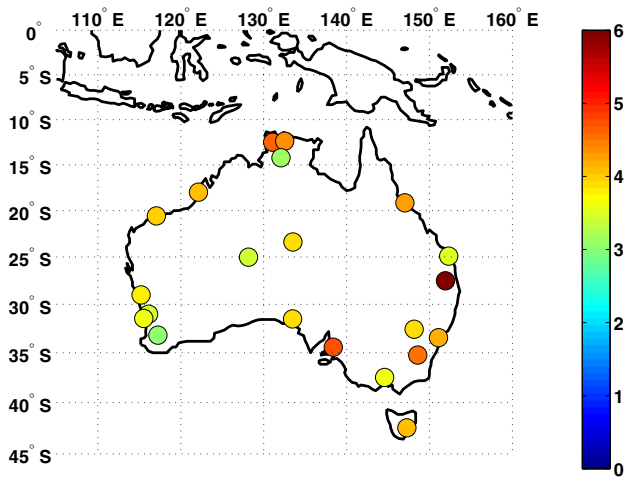


Fig. 8 Weighted standard deviations (in mm) of the vertical component of ANU GPS time series solutions after restoring IB-NTAL and removing a trend and a periodic signal and outliers

At this point, correcting the data for the IB-NTAL and D-NTOAL leads to a reduction of the weighted variance ranging between 3.0 and 52.5 % at 20 of the 21 considered sites (Table 3). Nine sites show a larger reduction by up to 6.7 % when D-NTOAL corrections are applied (Fig. 9). Applying IB-NTAL correction instead of D-NTOAL leads to 11 sites with similar changes showing a reduction of the weighted variance between -1 and 1 %. Only one site (BRO1) shows a reduction of 1.2 % larger with IB-NTAL correction applied. As expected from Sect. 2.4, the difference between correcting for IB-NTAL and D-NTOAL is small. The largest differences (≥ 2 %) occur along the southern coast at sites CEDU, ADE1, MOBS and HOB2 and at KARR and YAR2 on the northern and western coasts. We repeated the computations with the loading time series computed by van Dam et al. (2012) using the ECCO model (kf080) and obtain results that differ by ≤ 1.2 mm² (Table 3).

Table 3 Weighted variance of the Australian geodetic time series uncorrected (second column) and corrected for IB-NTAL (third column) and D-NTOAL (fifth and seventh columns using TUGO-m and ECCO models, respectively)

Site name	GPS (mm ²)	IB-NTAL		D-NTOAL				Δ	
		(mm ²)	(%)	TUGO-m		ECCO		TUGO-m	ECCO
				(mm ²)	(%)	(mm ²)	(%)	(%)	(%)
ADE1	21.2	17.6	16.9	16.2	23.7	16.8	20.6	6.8	3.7
ALIC	15.1	11.2	25.9	11.1	26.4	11.0	27.0	0.5	1.1
BNDY	12.4	11.3	8.8	11.4	7.9	12.6	-1.4	-0.9	-10.2
BRO1	16.6	17.1	-3.3	17.3	-4.5	-	-	-1.2	-
CEDU	14.6	10.0	31.5	9.4	35.3	10.1	30.8	3.8	-0.7
DARW	22.0	21.3	3.0	21.2	3.6	21.2	3.6	0.6	0.6
HOB2	15.8	14.6	7.6	14.3	9.6	14.3	9.6	2.0	2.0
JAB1	18.8	17.9	4.7	17.5	6.6	-	-	1.9	-
KARR	15.8	13.6	14.0	13.1	16.9	12.7	19.9	2.9	5.9
KAT1	9.9	8.8	10.7	8.8	10.7	-	-	0.0	-
MOBS	11.5	7.6	34.3	7.2	37.3	7.3	36.3	3.0	2.0
NNOR	11.7	7.9	32.1	8.1	31.2	7.9	32.1	-0.9	0.0
PARK	15.2	10.7	29.5	10.7	29.5	10.9	28.6	0.0	-0.9
PERT	13.1	10.6	19.3	10.4	20.7	10.5	19.6	1.4	0.3
SYDN	17.0	12.9	24.1	12.8	24.7	12.9	24.1	0.6	0.0
TIDB	20.4	16.3	20.2	16.1	21.1	16.2	20.5	0.9	0.3
TOOW	37.8	31.0	18.0	30.3	19.8	-	-	1.8	-
TOW2	18.4	17.7	4.3	17.7	4.3	18.6	-1.3	0.0	-5.6
WARA	11.7	7.0	40.3	7.1	39.6	-	-	-0.7	-
WAGN	9.5	4.5	52.5	4.5	52.5	-	-	0.0	-
YAR2	14.5	12.7	12.4	12.4	14.4	12.3	15.3	2.0	2.9

Standard deviations corresponding to the second column are plotted in Fig. 8. The differences of weighted variance reduction Δ (in %) between correcting geodetic time series for D-NTOAL, using TUGO-m and ECCO models, and IB-NTAL are in the ninth and tenth columns, respectively; those using TUGO-m are also plotted in Fig. 9

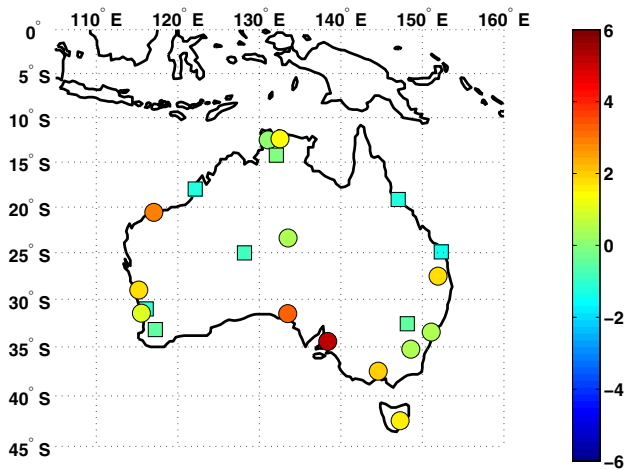


Fig. 9 Differences of the weighted variance reduction (in %) between correcting the vertical component of ANU GPS time series solutions for D-NTOAL and IB-NTAL. Circles are squares are for positive and negative values, respectively

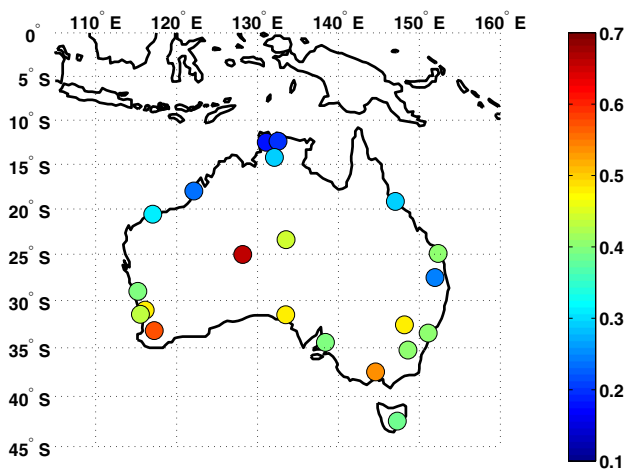


Fig. 10 Ratio of the weighted standard deviations of the vertical component of the displacement of Australian geodetic stations induced by D-NTOAL with that of ANU GPS time series solutions

To examine the importance of the predicted D-NTOAL with respect to the observed signal, we compute the ratios of the weighted variance of the predicted D-NTOAL time series with that of the uncorrected geodetic time series (Fig. 10). This ratio is a proxy for signal-to-noise ratio noting that a range of residual phenomena may contribute to the noise component. Therefore, a ratio close to one indicates that the predicted D-NTOAL variations are as large as those of the observed signal but do not imply a high correlation. In this case, correcting geodetic time series for D-NTOAL may lead to a better reduction of the weighted variance. Ratios range between 0.18 and 0.65. Two sites have a ratio larger than 0.5, eight have a ratio between 0.4 and 0.5, five between 0.3 and 0.4, five between 0.2 and 0.3 and only one site has a ratio lower than 0.2. The lowest ratios (<0.3) are obtained on the northern coast while at ADE1, CEDU, MOBS, HOB2

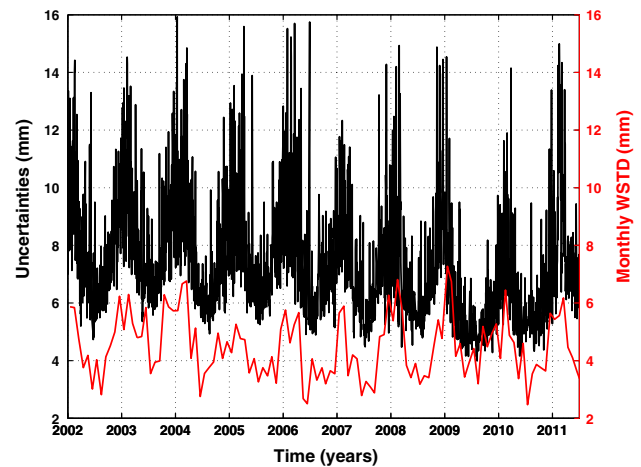


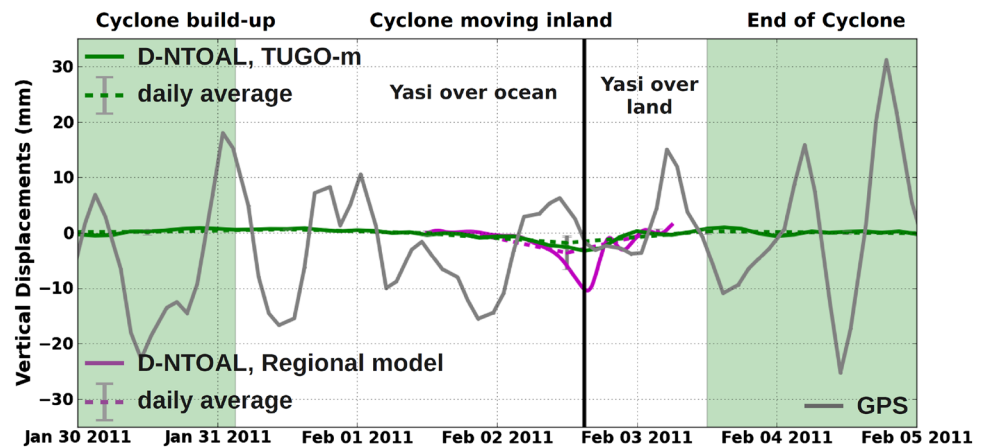
Fig. 11 Uncertainties (black) and monthly weighted standard deviation (WSTD, red) of the vertical displacement of TOW2 GPS site as a function of time (in mm)

and YAR2, the ratios are larger than 0.3. This may explain why the D-NTOAL correction at the northern sites does not outperform the IB-NTAL correction, despite these sites being subject to more rapid variations than those predicted by the IB assumption (Figs. 1b, 2).

In the three cases (D-NTOL, D-NTOAL, IB-NTAL) presented in Fig. 4, the daily-averaged deformation induced by cyclone Yasi is small (≤ 3 mm, Table 2) and difficult to discern from typical synoptic-scale temporal variability. The sub-daily scatter of the D-NTOL, D-NTOAL (considering TUGO-m) and IB-NTAL time series is 1.3, 1.0 and 0.4 mm, respectively. Inspection of Fig. 7 shows that the amplitude of the daily averages and their sub-daily scatters can be as large as 6.0 and 3.9 mm respectively for D-NTOL and 3.6 and 3.1 mm for D-NTOAL (if the high-resolution ocean model is considered, Table 2) noting again the counter acting effect of the atmospheric and oceanic loading signals. This implies that TUGO-m may not be accurate enough to correct for daily D-NTOAL that deviates from the IB-NTAL due to sub-daily ocean dynamics. Alternatively, the weighted standard deviation (WSTD) of the observed vertical displacement on the northern coast of Australia, where storm surge events are frequent, is larger than 4 mm (Fig. 8). This suggests that a cyclone-induced storm surge loading might not be detectable using daily GPS solutions at the present time.

Comparing the daily geodetic time series at TOW2 with the predicted D-NTOAL (not shown) confirms that no surge loading can be detected. Computing monthly WSTD of that time series (Fig. 11) shows seasonal signal (also observed at KARR and DARW) with WSTD values reaching more than 6 mm during the austral summers, corresponding to the tropical cyclone season, indicating a higher variability than during the austral winters. Therefore, the combination of a larger scatter of daily position estimates during the cyclone

Fig. 12 Observed and estimated (D-NTOAL) vertical displacement at TOW2



season and the low daily vertical displacement generated by a storm surge averaged over 24 h explains why we are not able to detect the single storm surge signature in the daily GPS time series observed at TOW2. However, given that the predicted magnitude of the vertical displacement due to D-NTOAL at TOW2 is about 10 mm within a day, we may be able to detect the storm surge event in sub-daily geodetic time series. We further investigate this point in the next section.

4.3 Sub-daily GNSS detection of cyclone-induced storm surges

Using a set of 26 GPS stations [Geng et al. \(2012\)](#) successfully detected sub-daily motions induced by a storm surge that occurred on the North Sea in November 2007. We investigate the detection of the surge developed during the tropical cyclone Yasi using TOW2, the closest GPS station to the surge and our sole continuously operating station in this region.

We use the GPS Inferred Positioning System/Orbit Analysis and Simulation Software (GIPSY/OASIS 6.2) package to undertake GPS analysis in a Precise Point Positioning (PPP) mode ([Zumberge et al. 1997](#)). Our processing strategy is similar to that of [Geng et al. \(2012\)](#) and we apply the same corrections described in Sect. 4.1. We use 5-min data to estimate 2-hourly positions as random walk parameters with $1 \text{ cm}/\sqrt{h}$ sigmas for the X , Y and Z components. To compare our processing strategy with that of [Geng et al. \(2012\)](#) we estimate the vertical displacement of WSRT and DELF stations adjacent to the North Sea. There, [Geng et al. \(2012\)](#) obtained an RMS of 7.8 and 10.7 mm respectively for data acquired in November 2007. Using the same gaussian filtering ($\sigma = 1$) we obtain 6.8 and 9.3 mm, respectively. We are also able to detect the signature of the storm surge that occurred on November 9 in the DELF time series, confirming that similar accuracy is achieved with our processing strategy. Processing TOW2 from January 6 to February 5 2011, we obtain an RMS of 16.4 mm. This reflects that, for a similar

time interval, TOW2 is noisier than WSRT and DELF. This can be further illustrated by comparing the RMS before and after applying the gaussian filter. Indeed, while the RMS at WSRT and DELF reduces by 2.1 mm after filtering, it reduces by 5.1 mm at TOW2. Reducing the time interval to January 24–February 5 2011, around the time of Yasi, decreases the RMS at TOW2 to 11.0 mm, with the filtering counting for 5.5 mm of this reduction.

Analysis of the TOW2 sub-daily GPS time series confirms that the series is dominated by quasi-diurnal noise and no significant deformation can be inferred during the passage of Yasi (Fig. 12). Unfortunately, detection of sub-daily signals of less than 15 mm in such a single and noisy GPS vertical time series remains an important challenge given the noise characteristics that remain in the current time series. TOW2 is located in a tropical region that is likely subject to different atmospheric effects compared with sites around the North Sea. Figure 11 shows the uncertainties of the daily vertical displacement of TOW2 as a function of time. It clearly shows an increase by more than 6 mm between the winter and summer seasons which we attribute to likely increased atmospheric turbulence. A network of stations in this region would help refine the GPS processing and detection of a common mode regional signature as induced by a storm surge ([Geng et al. 2012](#)).

5 Concluding remarks

We investigated the space and time signature at Australian geodetic sites of the differences between modelled NTOAL computed using the dynamic ocean model TUGO-m, which captures the high-frequency changes in the ocean, and the NTAL assuming that the ocean's response to atmospheric changes is an inverted barometer. We show that high-frequency ocean changes can lead to long-term scatter of predicted daily-averaged data that are 20–25 % larger in the D-NTOAL than in the IB-NTAL time series at four sites

(KARR, BRO1, TOW2, BNDY) along the northern coast of Australia. We also show that the long-term scatter of the IB-NTAL and D-NTOAL due to sub-daily ocean changes is significantly different in the northern and most of the southern coastal regions of Australia. These differences characterized the variations in the bathymetry along the Australian coast, reflecting that high-frequency ocean changes are larger in shallow water regions.

Analysis of daily GPS coordinate time series showed that a posteriori correction for D-NTOAL and IB-NTAL reduce the weighted variance at almost all sites (20/21). Nine sites (43 %) show a larger reduction after applying the D-NTOAL corrections. The largest reduction was found along the southern Australian coast, in contrast to our expectation of greater influence of the D-NTOAL in northern Australia (Fig. 2). There the observed scatter is lower, and predicted scatter higher than those of the northern coast. It is also likely that this relates to the complex interaction with hydrologically induced loading prevalent across northern Australia (Tregoning et al. 2009). The use of either TUGO-m or ECCO leads to very similar results suggesting that around Australia there is very little difference between these models at daily periods. However, small differences between these models remain difficult to accurately assess given the noise level in the daily GPS time series.

To determine an upper bound on D-NTOL and D-NTOAL in Australia we investigated one major storm surge event. We looked at the effect on the vertical displacement of the tropical cyclone Yasi that produced a storm surge of several metres on the eastern coast between Townsville and Cardwell. During the passage of Yasi, the D-NTOAL and D-NTOL at the Townsville GPS site TOW2 predicted by the regional model reach 10.4 and 14 mm respectively with more than 96 and 76 % of the displacement occurring within 15 h. The predicted vertical displacement due to D-NTOAL and D-NTOL obtained with TUGO-m at Townsville is just 3.2 and 4.6 mm, respectively. This displacement is likely underestimated given that the D-NTOAL and D-NTOL predicted using the TUGO-m model is less than one-third of that obtained using the surge component of the regional model. Nevertheless, both modelling results show that, during the storm surge, oceanic and atmospheric loading compensate and that the D-NTOL dominates and accounts for 135–140 % of the D-NTOAL. Also important for placing an upper bound on future surge events and their impact on GNSS time series, we showed that a maximum D-NTOAL and D-NTOL displacement of 14.0 and 16.5 mm in 15 h was predicted for the Yasi event from the regional model, coinciding spatially with Lucinda Jetty (18° 31' 26''S, 146° 19' 51''E).

The 10.4-mm vertical displacement predicted at the sole continuous GPS in the region (TOW2) due to D-NTOAL is less than half the 26–28 mm recorded at GORE, LOWE and ALDB GPS sites located in a similar geographical context in

England, during a large storm surge event in the North Sea (Geng et al. 2012). This undoubtedly reflects the difference in the coastline geometries between the embayment of the North Sea and the quasi-linear Australian coast that results in a faster dissipation of the load signal.

Regardless, the short time span in which the change occurs suggests that the amplitude is too low for a possible detection with existing GNSS analysis strategies, given the precision of the current daily-averaged and sub-daily geodetic time series. Investigating the daily GPS solutions updated from Tregoning and Watson (2009) showed that the daily-averaged D-NTOAL from this single event was too small (3.6 mm) to be detected (observed weighted standard deviation is 4.5 mm). It is also likely that the important sub-daily loading propagates in a complex way throughout the 24-h session defined in the GPS analysis (e.g. Penna et al. 2007). Processing sub-daily GPS data, we obtain similar precision as that of Geng et al. (2012) for two of their studied sites (i.e. DELF and WSRT) that would make the surge loading detection possible. However, the noise, attributed to atmospheric turbulence, is too high at TOW2 to perform such a detection. At the location of the maximum loading displacement, we speculate that the signal (14 mm) would just be observable above the noise within current sub-daily GNSS processing.

Haigh et al. (2014b) analysed the non-tidal component of the 30 tide gauge records along the Australian coast of which 10 are located on the northern coast, above 25°S. They identified the 100 largest storm surge events for the 10 northern sites with observing spans mostly longer than 30 years (1970–2008) and found that, for 7 of the 10 sites, the largest storm surge event was generated by a tropical cyclone and that the largest surge height was 2.84 m in Townsville. The following largest surges occurred in Broome (2.26 m) and Port Headland (2.06 m), indicating that we can expect similar D-NTOAL effects to that obtained at TOW2 for Yasi anywhere else along the northern Australian coast. Therefore, coastal GNSS sites above 25°S are likely to experience deformations at the ~15 mm level. Given the high-frequency nature of these signals, modelling using a dynamic ocean model rather than a simple IB assumption is required. The seasonal decrease in GPS time series precision that precludes detection of signals at this level along the northern Australian coast warrants further investigation.

Acknowledgments A. Mémin was supported by an Australian Research Council Super Science Fellowship (FS110200045). We thank the International GNSS Service and Geoscience Australia for making the GPS data used in this study freely available. The GPS data were computed on the Terrawulf II computational facility at the Research School of Earth Sciences, a facility supported through the AuScope initiative. AuScope Ltd. is funded under the National Collaborative Research Infrastructure Strategy (NCRIS), an Australian Commonwealth Government Programme. The authors thank F. Lyard and J.-P. Boy for providing the grids of the hydrodynamic Toulouse Unstructured Grid Ocean model. We also thank T. Van Dam for providing

the loading time series computed using the ECCO model. The authors acknowledge comments from two anonymous reviewers, T. Van Dam and S. Williams.

References

- Boy JP, Hinderer J, Gegout P (1998) Global atmospheric loading and gravity. *Phys Earth Planet Int* 109:161–177
- Boy JP, Lyard F (2008) High-frequency non-tidal ocean loading effects on surface gravity measurements. *Geophys J Int* 175:35–45. doi:10.1111/j.1365-246X.2008.03894.x
- Boy JP, Longuevergne L, Boudin F, Jacob T, Lyard F, Llubes M, Florsch N (2009) Modelling atmospheric and induced non-tidal oceanic loading contributions to surface gravity and tilt measurements. *J Geodyn* 48:182–188. doi:10.1016/j.jog.2009.09.022
- Bruinsma S, Lemoine JM, Biancale R, Valès N (2010) CNES/GRGS 10-day gravity field models (release 2) and their evaluation. *Adv Space Res* 45:587–601
- Carrère C, Lyard F (2003) Modelling the barotropic response of the global ocean to atmospheric wind and pressure forcing: comparisons with observations. *Geophys Res Lett* 30(6):1275. doi:10.1029/2002GL016473
- Coleman R, Dickey JM, Featherstone W, Higgins M, Johnston G, Lambbeck K, Lovell JEJ, McQueen H, Rizos C, Tingay S, Tregoning P, Twilley C, Watson CS (2008) New geodetic infrastructure for Australia. *J Spat Sci* 53(2):65–80
- Dee DP, Uppala SM, Simmons AJ, Berrisford P, Poli P, Kobayashi S, Andrae U, Balmaseda MA, Balsamo G, Bauer P, Bechtold P, Beljaars ACM, van de Berg L, Bidlot J, Bormann N, Delsol C, Dragani R, Fuentes M, Geer AJ, Haimberger L, Healy SB, Hersbach H, Hólm EV, Isaksen I, Kållberg P, Köhler M, Matricardi M, McNally AP, Monge-Sanz BM, Morcrette JJ, Park BK, Peubey C, de Rosnay P, Tavolato C, Thépaut JN, Vitart F (2011) The ERA-Interim reanalysis: configuration and performance of the data assimilation system. *Quart J Royal Meteor Soc* 137(656):553–597. doi:10.1002/qj.828
- Dziewonski AM, Anderson DL (1981) Preliminary reference Earth model. *Phys Earth Planet Int* 25:297–356
- Farrell WE (1972) Deformation of the Earth by surface loads. *Rev Geophys Space Phys* 10:761–797
- Fratepietro F, Baker TF, Williams SDP, Van Camp M (2006) Ocean loading deformations caused by storm surges on the northwest European shelf. *Geophys Res Lett* 33(6). doi:10.1029/2005GL025475
- Geng J, Williams SDP, Teferle FN, Dodson AH (2012) Detecting storm surge loading deformations around the southern North Sea using subdaily GPS. *Geophys J Int* 191(2):569–578. doi:10.1111/j.1365-246X.2012.05656.x
- Haigh ID, Wijeratne EMS, MacPherson LR, Pattiaratchi CB, Mason MS, Crompton RP, George S (2014a) Estimating present day extreme water level exceedance probabilities around the coastline of Australia: tides, extra-tropical storm surges and mean sea level. *Clim Dyn* 42:139–147. doi:10.1007/s00382-012-1652-1
- Haigh ID, MacPherson LR, Wijeratne EMS, Mason MS, Pattiaratchi CB, Crompton RP, George S (2014b) Estimating present day extreme water level exceedance probabilities around the coastline of Australia: tropical cyclone-induced storm surges. *Clim Dyn* 42:121–138. doi:10.1007/s00382-012-1653-0
- Herring TA, King RW, McClusky SC (2010) Introduction to GAMIT-GLOBK. Massachusetts Institute of Technology, Cambridge pp 48
- Kalnay E, Kanamitsu M, Kistler R, Collins W, Deaven D, Gandin L, Iredell M, Saha S, White G, Woollen J, Zhu Y, Leetmaa A, Reynolds R, Chelliah M, Ebisuzaki W, Higgins W, Janowiak J, Mo K, Ropelewski C, Wang J, Jenne R, Joseph D (1996) The NCEP/NCAR 40-year reanalysis project. *Bull Am Meteor Soc* 77:437–470
- Lemoine JM, Bruinsma S, Loyer S, Biancale R, Marty JC, Perosanz F, Balmino G (2007) Temporal gravity field models inferred from GRACE data. *Adv Space Res* 39:1620–1629. doi:10.1016/j.asr.2007.03.062
- Mémin A, Rogister Y, Hinderer J, Llubes M, Berthier E, Boy JP (2009) Ground deformation and gravity variations modelled from present-day ice thinning in the vicinity of glaciers. *J Geodyn* 48(3–5):195–203. doi:10.1016/j.jog.2009.09.006
- Merriam JB (1992) Atmospheric pressure and gravity. *Geophys J Int* 109:488–500
- Penna NT, King MA, Stewart MP (2007) GPS height time series: short-period origins of spurious long-period signals. *J Geophys Res* 112(B2). doi:10.1029/2005JB004047
- Petit G, Luzum B (2010) IERS Conventions (2010). IERS Technical note no 36, Verlag des Bundesamts für Kartographie und Geodäsie Frankfurt am, Main, pp 179
- Petrov L, Boy J (2004) Study of the atmospheric pressure loading signal in very long baseline interferometry observations. *J Geophys Res-Solid Earth* 109(B03405). doi:10.1029/2003JB002500
- Ray J, Altamimi Z, Collilieux X, van Dam T (2008) Anomalous harmonics in the spectra of GPS position estimates. *GPS Solut* 12:55–64. doi:10.1007/s10291-007-0067-7
- Schuh H, Estermann G, Crétaux JF, Bergé-Nguyen M, van Dam T (2003) Investigation of hydrological and atmospheric loading by space geodetic techniques. IAG Proc 126:123–132 Hwang C, Shum CK, Li JC (eds) International Workshop on Satellite Altimetry
- Stammer D, Wunsch C, Fukumori I, Marshall J (2002) State estimation in modern oceanographic research. *Eos Trans AGU* 83(27):294–295. doi:10.1029/2002EO000207
- Tierney C, Wahr J, Zlotnicki V (2000) Short-period oceanic circulation: implications for satellite altimetry. *Geophys Res Lett* 27:1255–1258
- Tregoning P, van Dam TM (2005) Atmospheric pressure loading corrections applied to GPS data at the observation level. *Geophys Res Lett* 32(22). doi:10.1029/2005GL024104
- Tregoning P, Watson C (2009) Atmospheric effects and spurious signals in GPS analyses. *J Geophys Res* 114(39). doi:10.1029/2009JB006344
- Tregoning P, Watson C (2011) Correction to atmospheric effects and spurious signals in GPS analyses. *J Geophys Res* 116(B2). doi:10.1029/2010JB008157
- Tregoning P, Watson C, Ramillien G, McQueen H, Zhang J (2009) Detecting hydrologic deformation using GRACE and GPS. *Geophys Res Lett* 36(15). doi:10.1029/2009GL038718
- van Dam TM, Wahr JM (1987) Displacements of the Earth's surface due to atmospheric loading: effects on gravity and baseline measurements. *J Geophys Res* 92(B2):1281–1286
- van Dam TM, Herring TA (1994) Detection of atmospheric pressure loading using very long baseline interferometry measurements. *J Geophys Res* 99(B3):4505–4517
- van Dam TM, Blewitt G, Heflin MB (1994) Atmospheric pressure loading effects on global positioning system coordinate determinations. *J Geophys Res* 99(B12):23939–23950
- van Dam TM, Collilieux X, Altamimi Z, Ray J (2012) Nontidal ocean loading: amplitudes and potential effects in GPS height time series. *J Geod* 86(11):1043–1057. doi:10.1007/s00190-012-0564-5
- Williams SDP, Penna NT (2011) Non-tidal ocean loading effects on geodetic GPS heights. *Geophys Res Lett* 38(9). doi:10.1029/2011GL046940
- Wunsch C (1972) Bermuda sea level in relation to tides, weather, and baroclinic fluctuations. *Rev Geophys* 10:1–49
- Wunsch C, Stammer D (1997) Atmospheric loading and the oceanic inverted barometer effect. *Rev Geophys* 31:79–107
- Zumberge JF, Heflin MB, Jefferson DC, Watkins MM, Webb FH (1997) Precise point positioning for the efficient and robust analysis of GPS data from large networks. *J Geophys Res* 102(B3):5005–5017. doi:10.1029/96JB03860